C. R. Mecanique 346 (2018) 98–109

Contents lists available at ScienceDirect

Comptes Rendus Mecanique

www.sciencedirect.com

Limit analysis, rammed earth material and Casagrande test

Ranime El-Nabouch [a], Joseph Pastor [a,*], Quoc-Bao Bui [a,b], Olivier Plé [a]

[a] Université Savoie Mont Blanc, CNRS, LOCIE, 73000 Chambéry, France
[b] Ton Duc Thang University, Faculty of Civil Engineering, Ho Chi Minh City, Viet Nam

ARTICLE INFO

Article history:
Received 8 May 2017
Accepted 22 November 2017
Available online 4 January 2018

Keywords:
Limit analysis
Lower and upper bound methods
Cohesive Cam–Clay material
Micromechanics identification
Casagrande geotechnical test
Conic programming

ABSTRACT

The present paper is concerned with the simulation of the Casagrande test carried out on a rammed earth material for wall-type structures in the framework of Limit Analysis (LA). In a preliminary study, the material is considered as a homogeneous Coulomb material, and existing LA static and kinematic codes are used for the simulation of the test. In each loading case, static and kinematic bounds coincide; the corresponding exact solution is a two-rigid-block mechanism together with a quasi-constant stress vector and a velocity jump also constant along the interface, for the three loading cases. In a second study, to take into account the influence of compressive loadings related to the porosity of the material, an elliptic criterion (denoted Cohesive Cam–Clay, CCC) is defined based on recent homogenization results about the hollow sphere model for porous Coulomb materials. Finally, original finite element formulations of the static and mixed kinematic methods for the CCC material are developed and applied to the Casagrande test. The results are the same than above, except that this time the velocity jump depends on the compressive loading, which is more realistic but not satisfying fully the experimental observations. Therefore, the possible extensions of this work towards non-standard direct methods are analyzed in the conclusion section.

1. Introduction

Earth materials have been attracting numerous scientific researches because of the low embodied energy and of a positive hygrothermal behavior. The present paper deals with the simulation of the Casagrande test carried out in our laboratory on a rammed earth material denoted “pisé” in French. The novelty of this study concerns the use of both Limit Analysis (LA) methods, firstly when considering the material as obeying the Coulomb criterion, and secondly when using a homogenization model for porous materials to define an elliptical criterion (of Cam–Clay type) in an attempt to better represent the earth material for finite structures such walls; in each case, the behavior of the material in the experimental tests is analyzed by *ad hoc* finite element modelings. All resulting codes lead to conic optimization problems solved with the MOSEK commercial code. It is worth noting here that numerical and analytical solutions about direct computation of limit loads (i.e. in the LA framework) with Cam–Clay-type criteria do not exist in the literature, at least up to our knowledge.

The paper is organized as follows. First, the results of a preliminary study, where the rammed earth is considered as a homogeneous Coulomb material and by using existing LA codes, are briefly presented. For all loading cases, the final static

* Corresponding author.
E-mail address: joseph.pastor@univ-smb.fr (J. Pastor).

https://doi.org/10.1016/j.crme.2017.11.007

and kinematic approaches give quasi-identical results in terms of loading parameters, with a two-rigid block kinematic solution with a constant velocity jump, and a quasi-constant stress vector along the shearing plane. However, the observed dilatancy is not depending on the intensity of the vertical loading for a given velocity on the lower half-box: such a feature does not seem realistic when considering homogenization results for materials with a non-negligible porosity.

In a second part, to take into account this porous character, an elliptic criterion, here denoted Cohesive Cam–Clay criterion (CCC), is defined on the basis of the homogenization approach called the hollow sphere model of references [1], [2], and [3]. In the last section, original static and kinematic LA codes are developed for this CCC criterion and used for the shear test problem, the corresponding results being discussed in the final part of the paper.

2. The Limit Analysis methods, briefly

The Limit Analysis theory aims to determine the limit loads of a material system that obeys a criterion of convex plasticity and the associated flow rule. This theory allows obtaining a framework for these limit loads via two separate approaches and a mixed approach. For the two separate approaches, the first method, or static method, provides a lower bound of the limit load. The second method, called kinematic (classical), gives an upper bound. The first one contains only the stresses as variables, and the second one only the velocities. The mixed approach involves both types of variables and requires only the expression of the plasticity criterion as a characteristic of the material. In addition, under certain conditions verified here, it also leads to rigorous upper bounds.

After discretization of the mechanical system in finite elements, the resulting problems lead to optimize a linear functional under linear and convex constraints. Since the early 2000s, the conic optimization codes (such as MOSEK, [4]) made it possible to solve directly these non-linear optimization problems with a very good efficiency. In the present paper, the MOSEK conic code is also used for solving the problems arising from an improved version of the criterion proposed in [2], first for identifying the criterion itself, then for the FEM simulations of the experimental tests.

3. The Casagrande test and its preliminary modelization as a Coulomb material: results

This section aims to present the mechanical and numerical environment available to simulate the shear test with the Casagrande box (Fig. 1), for the Coulomb material. The presentation of the experimental apparatus, too long to be detailed here, can be found in references [5,6].

3.1. Mechanical modeling of the Casagrande test

Schematically, the test (cf. Fig. 1, left) consists in applying a vertical force N by means of a metallic plate, and the shearing at the interface of the two metal half-boxes (of square section) is carried out via the horizontal displacement of the lower half-box. The upper half-box is horizontally blocked. The lower half-box is laid on rollers in order to make the sliding resistance negligible. In the figure is plotted the median section of the apparatus, where metal parts are in black and Teflon in green. The horizontal velocity V, here positive, of the lower half-box (A′B′C′D′) is noted V_F in the following, and the shear plane is noted GH.

Taking into account that the vertical parts and the bottom of the box are provided with a thin Teflon layer, it can be assumed that the corresponding interfaces (EG, FH and GIJH in the figure) are smooth. The metal parts of the box are undeformable compared to the material, which is assumed homogeneous and isotropic. The displacement of the box on the z axis is zero, and the axial load N is applied in the middle of the upper plate. Due to the symmetries and the boundary conditions of the problem, a plane strain approach is used, where the (x, y) plane is that of the figure, with the velocity field in the material $(u_x(x, y), u_y(x, y), u_z = 0)$. For the present problem, the extension of the stress field solution to the 3D case is easy (with $\tau_{yz} = \tau_{zx} = 0$, and $\sigma_z(x, y)$ only constrained by the plasticity criterion). Similarly, the displacement velocity field is directly extensible in 3D with $u_z(x, y) = 0$: the exact solution in 2D will also be exact from a three-dimensional point of view, and thus for the 3D test box.

As a consequence, Fig. 1 represents the plane strain test simulated in the context of the limit analysis. Let us assume *a priori* the Coulomb law of friction on the GH interface. Since the velocity jump in the tests is non-zero along GH, the relation $|\tau| = c - \sigma_n \tan\phi$ is verified (with positive traction stress, and c, ϕ constants); the equilibrium conditions of the two half-boxes (Fig. 1) classically give:

$$F = \int_{\mathrm{GH}} \tau_{nt}\,\mathrm{d}S = cL - \tan\phi \int_{\mathrm{GH}} \sigma_y\,\mathrm{d}S = cL + N\tan\phi \tag{1}$$

where L is the length of the segment GH, and F the force associated with the imposed velocity V_F. The Casagrande test returns directly the cohesion and the friction angle of the *a priori* assumed Coulomb criterion without any hypothesis about the plastic flow rule of the material. In terms of the LA static approach, since all the corresponding stress fields (including the one of the exact LA solution) must be statically admissible, these fields obey the local equilibrium conditions, and consequently the equilibrium of the parts, used above, is also satisfied; Relation (1) gives the exact LA solution *in terms of the loading parameters N and F*.

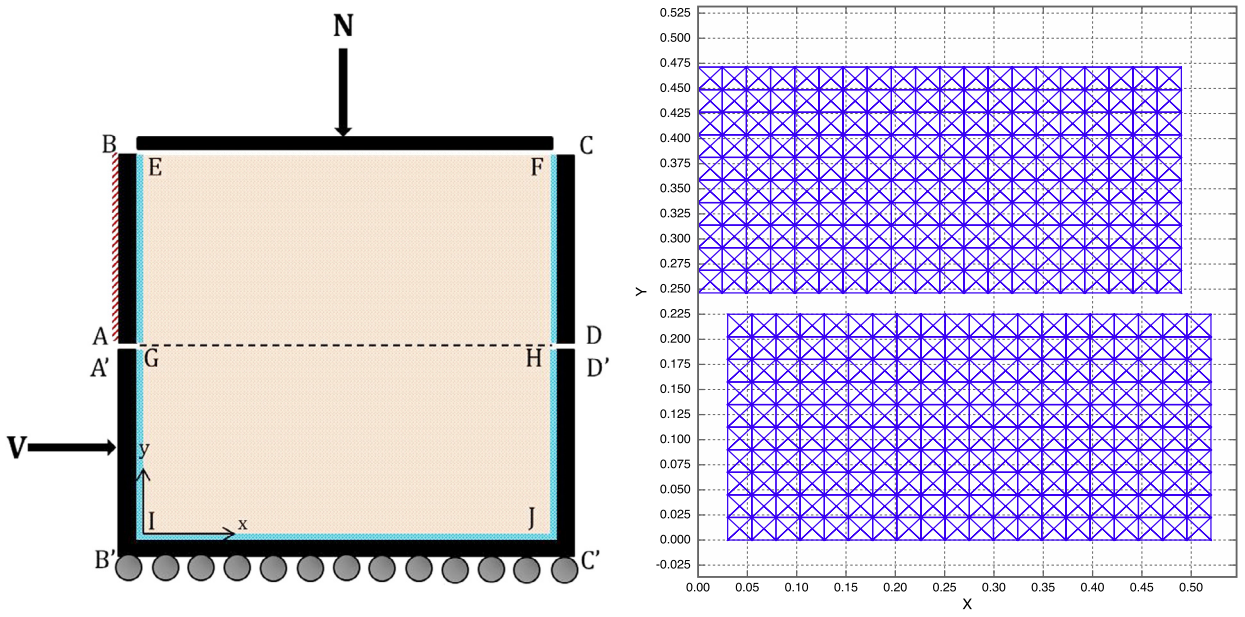

Fig. 1. Mechanical problem and deformed FEM meshes for Coulomb material.

Note that Equation (1) is easily obtained by using the LA kinematic theorem and the admissible two-rigid-block mechanism suggested in Fig. 1 right, with $[u_t] = V_F$ along GH and $P_{\text{ext}} = (F - N\tan(\phi))V_F = P_{\text{diss}} = c|[u_t]|L$. This confirms that Relation (1) gives the exact solution in terms of the loading parameters.

3.2. Numerical modelings

A discretization of the soil in 1600 triangular, *discontinuous*, elements is adopted, as in the deformed mesh of Fig. 1 right. This discretization is largely sufficient, since it leads to the quasi-coincidence of the lower and upper bounds as will be seen in the following. In the static code, to each vertex of the finite element are assigned the three components $(\sigma_x, \sigma_y, \tau_{xy})$ of the stress tensor, which varies linearly in the triangle; such a linearity condition is required to ensure that the plasticity criterion will be verified everywhere in the element.

In the classic kinematic code, to each vertex of the triangle is assigned a velocity vector (u_x, u_y) and the velocity field in the element is affine, the strain rate tensor is constant and the plastic admissibility verified within the element with one condition. Each inter-element side can be a discontinuity line: by imposing the plastic admissibility condition to the jump $[u_x, u_y]$ at each end, the flow rule is ensured all along the side because of the convexity of the set of the plastically admissible jumps, since the jump variation along the side is linear. In the same way, to represent the soil–metal interfaces, additional "vertices" are added in the metal in front of the corresponding vertices of the mesh.

By imposing the set of static and kinematic requirements in the soil and at the interfaces, the results are rigorous lower and upper bounds to the limit load of the problem studied. Solving the final problems of optimization needs less than one minute with the MOSEK optimizer. More details can be found for example in [7] for the static problem, and in [8] for the discontinuous kinematic approach with Coulomb as a special case.

3.3. Casagrande test with Coulomb material

In this section, the earth material obeys the Coulomb criterion. The cohesion $c = 0.0302$ MPa and the friction angle $\phi = 35.3°$ are obtained from the three experimental tests on the quasi-dry material (moisture content less than 3 %). Fig. 2 (with positive compression stress) gives these experimental results obtained with the shear apparatus where the lower half-box was in fact moved from right to left. Details about the experimental tests, for example about the graphs of shear force versus displacement of the lower half-box during the test—too long to be detailed here—can be found in [5] and in the recent thesis [6].

3.4. Numerical tests

In the following, the three experimental loadings (N, F)—named in this way since they are defined from the interpolation line of Fig. 2—are given in Table 1, for a 0.49 m length of GH (for a unit width along the z axis and for positive traction stresses).

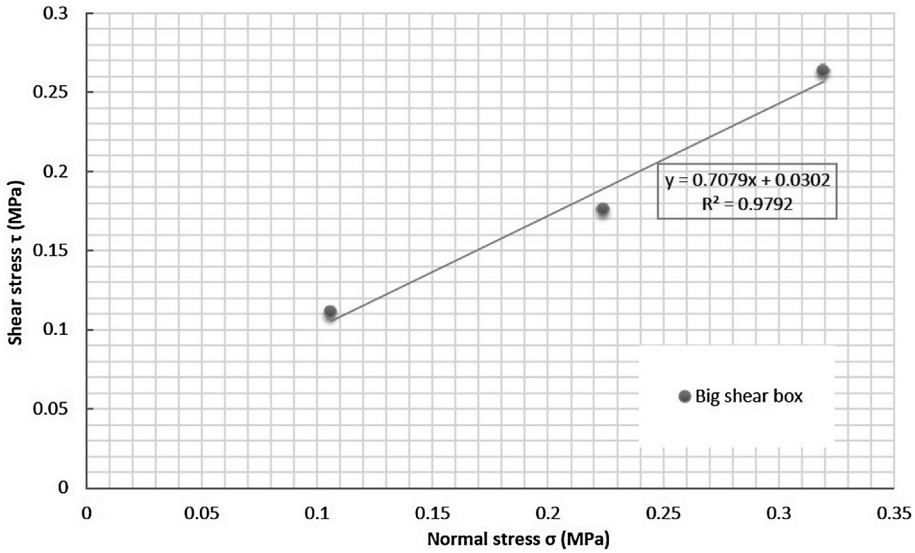

Fig. 2. Experimental results and the resulting interpolation line, after [5] and [6] (positive compression stress).

Table 1
Results from the three experimental tests.

Stress and load vectors	Test 1	Test 2	Test 3
σ_y^{d} (MPa)	−0.16	−0.24	−0.32
τ_{xy}^{d} (MPa)	−0.14346	−0.20010	−0.25673
N (kN)	78.4	117.6	156.8
F (kN)	70.3	98.05	125.8

- In each case, a unit velocity V_F is imposed on the lower box, and a vertical load N on the plate. The horizontal force associated with V_F is denoted as F and the LA problem involves here two loading parameters N and F. For the three tests, the numerical static and the kinematic forces F obtained are quasi-identical: the common value is confirmed as the exact solution in terms of loading parameters, and these common values are well practically the same than the loadings ones of Table 1. This is consistent with the fact that the plastic dissipation only occurs at the interface between the two parts, the volume strain rate remaining null in all triangles.
- Fig. 1 (right) illustrates the deformed meshes obtained for the material by using the kinematic approach, with an arbitrary graphic scale. This kinematics is strictly the same for each loading case, as expected since the two blocks remain rigid and the same velocity V_F is imposed on the lower half-box: $\tan\phi$ is also the ratio of the normal and tangential displacement jumps for any point along GH.
- As a confirmation, in the static solution, the plasticity criterion is zero only along the interface. For the three loadings N_i, the stress vector is quasi-constant along the shear interface, including at the ends of GH (Fig. 1, right) owing to the stress discontinuities allowed at these ends; in the case N_2 for instance, the tangential stress τ_{xy} varies from −0.1998 to −0.2002 MPa (and the normal stress σ_{xy} from −0.2396 to −0.2400 MPa) along the 20 element sides of GH, values to be compared with those of Table 1.
  Let us recall that the stress field is unique only in the union of the deformed zones of the exact solution, i.e. only along the velocity discontinuity GH in the present case. Hence the stress field in the interior of both half-boxes, far from homogeneous, may not be representative of the actual field in the experiment. Taking into account that the convergence tolerance of the optimizer is fixed to 10^{-7} and that the admissibility conditions of the stresses are verified at a precision better than of 10^{-6}, this quasi-constancy of the stress vector along the interface is significant. Up to our knowledge, this constancy and the exact character solution, in the limit analysis framework, have not been pointed out previously in the literature.

To conclude with the case of the Coulomb material, the plastic flow, or the ruin of the system, is well obtained with the FEM codes for each loading case, but the experiments do not show such a rise of the upper box. Anyway, using the LA kinematic approach allows us to obtain true upper bounds for the collapse loads of real soil problems, from Radenkovic's theorems for non-standard materials.

On the other hand, the observed jump does not depend on the imposed loading N; this is hardly acceptable when considering that the earth material exhibits a porosity experimentally measured at 25% at Politecnico di Milano by mercury injection. Indeed, the LA pioneering paper of Gurson [9] and the subsequent works about the homogenization of porous

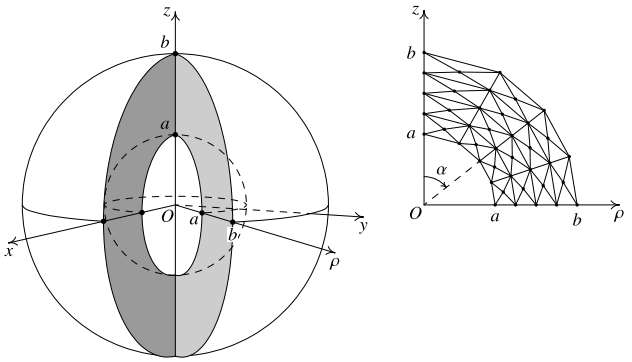

Fig. 3. The hollow sphere model and its FEM axisymmetric discretization.

materials in plasticity lead to a bounded convex criterion, therefore to a loading dependence for the macroscopic strain rate (and for the velocity jump on the discontinuities), at least in the limit analysis framework. As a consequence, the following study will use an elliptic approximation of the macroscopic criterion obtained with the hollow sphere model, i.e. the only homogenization model in plasticity, at least for the moment, which gives the macroscopic criterion for the porous Coulomb material (see [10] and [3]).

4. The hollow sphere model, briefly

Results of tests with isotropic loadings, especially in traction, are not easily available with the present material: this explains the use of the hollow sphere model for the analytical limit values for isotropic compression and traction given in [1], and for the numerical tools in [3]. Here we recall only the definition of the model and the corresponding macroscopic relations that will be used in the next sections. This model is made up of a spherical cavity embedded in a confocal spherical cell, with a Coulomb solid matrix. Fig. 3 presents the geometric model, where the porosity f allows one to determine the parameters a and b of the model.

Let us note Σ and D the macroscopic stress and strain rate tensors. These quantities are related to the microscopic fields by the averages over the model of volume V:

$$\Sigma_{ij} = \frac{1}{V}\int_V \sigma_{ij}\,\mathrm{d}V, \qquad D_{ij} = \frac{1}{2V}\int_{\partial V}(u_i n_j + u_j n_i)\,\mathrm{d}S \tag{2}$$

where u denotes the velocity vector and n the normal vector to the boundary ∂V of the model. Under the uniform strain rate boundary conditions, i.e. $u_i = D_{ij}x_j$ (where x represents the position vector), on the external boundary, the virtual dissipated power $P_{\mathrm{tot}} = V\,\Sigma_{ij}D_{ij}$ can be written as follows:

$$P_{\mathrm{tot}} = V\ Q\cdot\dot{q} \tag{3}$$

where the vector Q is the loading vector (4) and the vector $\dot{q}$ is the generalized velocity vector (5).

$$\begin{aligned} &Q_1 = \Sigma_{\mathrm{m}} = \frac{1}{3}\left(\Sigma_x+\Sigma_y+\Sigma_z\right), \quad Q_2 = \frac{\Sigma_x+\Sigma_y}{2} - \Sigma_z, \quad Q_3 = \frac{\sqrt{3}}{2}\left(\Sigma_x-\Sigma_y\right)\\ &Q_4 = \sqrt{3}\Sigma_{yz}, \quad Q_5 = \sqrt{3}\Sigma_{zx}, \quad Q_6 = \sqrt{3}\Sigma_{xy} \end{aligned} \tag{4}$$

$$\begin{aligned} &\dot{q_1} = D_x + D_y + D_z, \quad \dot{q_2} = \frac{2}{3}\left(\frac{D_x+D_y}{2} - D_z\right), \quad \dot{q_3} = \frac{1}{\sqrt{3}}\left(D_x - D_y\right)\\ &\dot{q_4} = 2D_{yz}/\sqrt{3}, \quad \dot{q_5} = 2D_{zx}/\sqrt{3}, \quad \dot{q_6} = 2D_{xy}/\sqrt{3} \end{aligned} \tag{5}$$

From isotropy and projection arguments, it can be proved that loadings can be restricted to the principal strain rates D as well as Σ, with $D_x = D_y$ and $\Sigma_x = \Sigma_y$; the final problem is axisymmetric and involves only two non-zero loading parameters, Q_1 and Q_2. Then, from the symmetries of the model, the quarter of the meridian plane of the hollow spheroid is meshed into triangular elements as shown in Fig. 3 right with a coarse mesh. In the present case, the following expression of the macroscopic equivalent stress Σ_{eq}, together with Σ_{m} above, will be used in the following:

$$\Sigma_{\mathrm{eq}} = \sqrt{\frac{3}{2}\,\Sigma' : \Sigma'} = \sqrt{Q_2^2 + Q_3^2} = |Q_2| \tag{6}$$

where Σ' is the deviatoric part of Σ. It is worth noting that, when expressed as $(\Sigma_{\mathrm{m}}, \Sigma_{\mathrm{eq}})$, the axisymmetric result is also an upper bound for the three-dimensional problem.

Table 2
Schematic constraint matrix of the identification problem.

	$p_0(\phi)$	$p_1(\phi)$	$\Sigma_{xx}, \Sigma_{yy}, ..., \Sigma_{xy}$	$Q_1 = p$	$Q_{i>1}$	x_1	x_2
Q_1 (4)			×	×			
$Q_{i>1}$ (4)			×		×		
x_1 (10.ii)	×			×		×	
x_2 (10.ii)		×		×			×
CCC (10)					×	×	×

5. The CCC criterion and its LA numerical implementation

5.1. The Cam–Clay criteria

The original Cam–Clay criterion [11] was defined to account for the possibility of plastic failure under compressive loading of pulverulent materials in geotechnics; it is strongly dissymmetric and presents a corner at the origin of the average stress axis. To circumvent the problems related to this corner, an elliptic formulation, called modified Cam–Clay criterion, has been proposed in [12], with the usual notations in geotechnics $q = \Sigma_{eq}$ and $p = \Sigma_m$:

$$q - M\sqrt{-p(p - p_1)} \leq 0; \quad M = 6\sin\phi/(3 - \sin\phi) \tag{7}$$

where p_1 is the compressive strength (here taken as negative) of the material under isotropic loading.

Both of these formulations are by no way adapted to cohesive materials, since the allowed average stress is only compressive ($p \leq 0$). To remove this drawback, the following "translated modified" formulation was proposed in [2], with c and ϕ being the cohesion and the friction angle of the (non-porous) matrix:

$$g(\sigma) = q - M\sqrt{(p_0 - p)(p - p_1)} \leq 0 \tag{8}$$

where the parameters p_0 and p_1 are the exact analytical solutions for a porous Coulomb material given in [1], in isotropic traction and compression, respectively:

$$p_0 = c\cot\phi\left[1 - f^{\frac{4}{3}\frac{\sin\phi}{1+\sin\phi}}\right]; \quad p_1 = c\cot\phi\left[1 - f^{-\frac{4}{3}\frac{\sin\phi}{1-\sin\phi}}\right] \tag{9}$$

where f is the porosity, and ϕ the *matrix* friction angle of the hollow sphere model. Note that a criterion of the form (8) was proposed from the modified Cam–Clay criterion to take into account the suction phenomenon for elastoplastic computations in [13] and [14].

5.2. Definition and identification of the CCC criterion

To complete the definition of the criterion (8), we need the cohesion c_m and the matrix friction angle ϕ_m of the hollow sphere model for the present soil. Also, to obtain an elliptic approximation of the criterion (denoted here Cohesive Cam–Clay, CCC) fully defined with the homogenization model, the parameter M will be numerically adjusted at the critical state (i.e. $\dot{q_1} = 0$ in (5)) so that the Σ_{eq} of the CCC criterion and of the homogenization model are the same ones by using (6) and the axisymmetric mixed code of [3], for a given couple of c_m and ϕ_m. In the following, we detail how obtaining the final couple (c_m, ϕ_m) so that the three loadings (N, F) of Table 1 just become admissible.

5.2.1. The identification process

In the reference [3], it can be seen that, for a given porosity f of the material, the pure shear strength is approximately constant for all friction angles ϕ_m, with the value $2c_m(1 - f)$, where c_m is the cohesion of the matrix; this point has been specifically verified here by varying the angle ϕ_m (for $\Sigma_m = 0$) with the axisymmetric mixed code. Hence, we define the matrix cohesion as $c_m = c_{exp}/(1 - f)$.

To obtain the best expression of the CCC criterion $g(\Sigma)$ compatible with the three test values, we need the criterion in the Mohr plane, i.e. $g_{nt}(\Sigma_n, \Sigma_{nt})$ on an arbitrary facet of normal n, owing to the isotropy of the CCC material. Hence we search for the projection of the CCC criterion $g(\Sigma)$ on the Mohr plane for a facet of GH to facilitate the comparison with the experimental and numerical results.

The parameter M of the CCC criterion is defined by using the mixed kinematic code of [3] as said above; then the CCC condition is written in the form called "rotated quadratic cone" by MOSEK:

$$\Sigma_{eq}^2 = \frac{3}{2}\Sigma' : \Sigma' = q^2 = Q_2^2 + Q_3^2 + Q_4^2 + Q_5^2 + Q_6^2 \leq 2x_1x_2 \tag{10.i}$$

$$x_1 = M(p_0 - p)/2 \geq 0; \quad x_2 = M(p - p_1) \geq 0 \tag{10.ii}$$

where Σ' is the deviatoric part of Σ, the Q_i defined in (4).

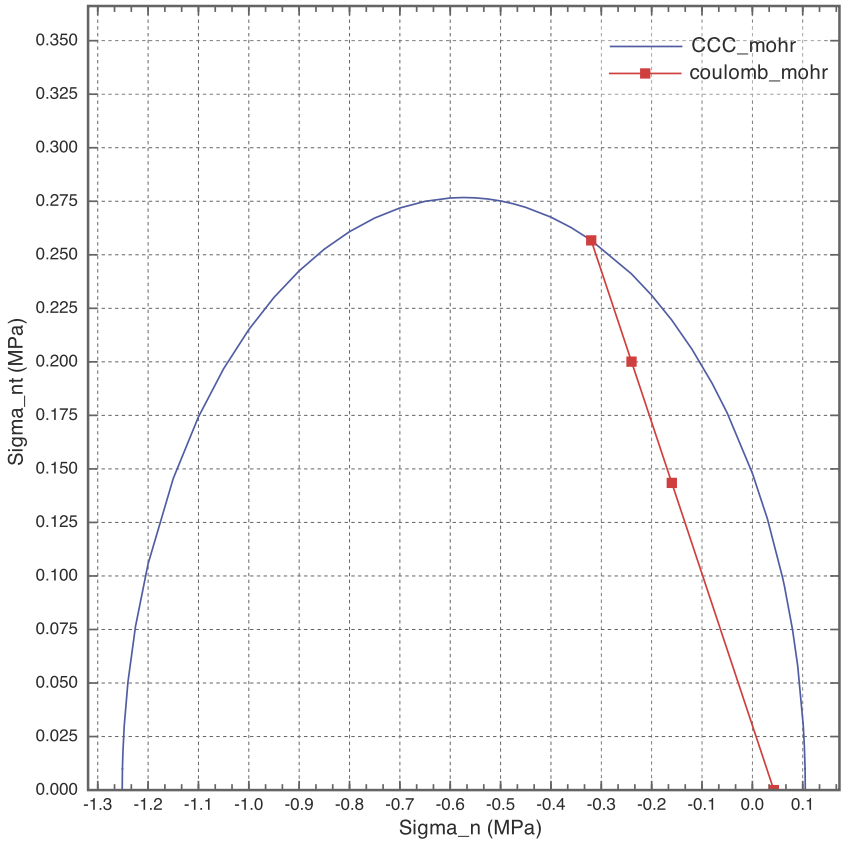

Fig. 4. The CCC criterion and the experimental Coulomb criterion in the Mohr plane.

Table 3
Comparison of limit stress vectors Coulomb/Cam–Clay in the Mohr plane.

Stress vector (MPa)	Test 1	Test 2	Test 3
σ_n^{d}	−0.16	−0.24	−0.32
τ_{nt} Coulomb	0.14346	0.20010	0.25673
τ_{nt} MCC	0.21948	0.24106	0.25675

The constraint matrix of the resulting conic optimization problem involves the equality constraints defining the variables Q_i from (4) and the two equalities for the definition of x_1 and x_2. The criterion is defined afterwards by listing the x_1, x_2 and Q_i variables of Relations (10) in the (extended) standard MPS file required by MOSEK. Table 2 schematically presents these constraints with the corresponding variables. For a given friction angle ϕ_{m} and the corresponding p_0 and p_1, the required projection is therefore easily obtained by maximizing Σ_{xy} $(= \Sigma_{nt})$ for given values of Σ_y $(= \Sigma_n)$ (or conversely), other Σ components free.

Then we consider the third loading case of Table 1, i.e. $\Sigma_y = \Sigma_n = -0.32$ MPa. Starting from ϕ_{exp}, ϕ_{m} is increased until the optimal functional Σ_{xy} just equals the corresponding test result (i.e. 0.25673 MPa given by the interpolation line in Fig. 2), with $\phi_{\mathrm{m}} = 39.418°$ and $M = 0.80126$ as final results. In a second step, with these parameter values, we maximize Σ_y for a zero value of Σ_{xy} to obtain the point on the Σ_n axis, with the result $\Sigma_n = 0.10509$ MPa.

Since the maximal isotropic Coulomb traction ($H = c/\tan\phi = 0.04265$ MPa) is lower, owing to the convexity of the criterion and the linearity of the Coulomb relation, all intermediate Coulomb loadings are admissible, as it can be seen in Fig. 4, where the corresponding three test values are reported, together with the CCC criterion in the Mohr plane. For comparison with the MEF results of the next section, Table 3 gives the limit values of the stress vector for both criteria.

Finally, the CCC criterion is fully defined from the hollow sphere model by (8) and (9) with $p_0 = 0.02509$ MPa, $p_1 = -1.17139$ MPa, and $M = 0.80126$. In Fig. 5, this criterion is plotted with the porous Coulomb criterion obtained with the axisymmetric mixed code. It can be seen that the MCC criterion is a good elliptic approximation of the solution to the homogenization problem compatible with the exact isotropic values (9) and with the available experimental data. The reader is referred to [3] for a full description of the hollow sphere model and its numerical approaches in the LA framework.

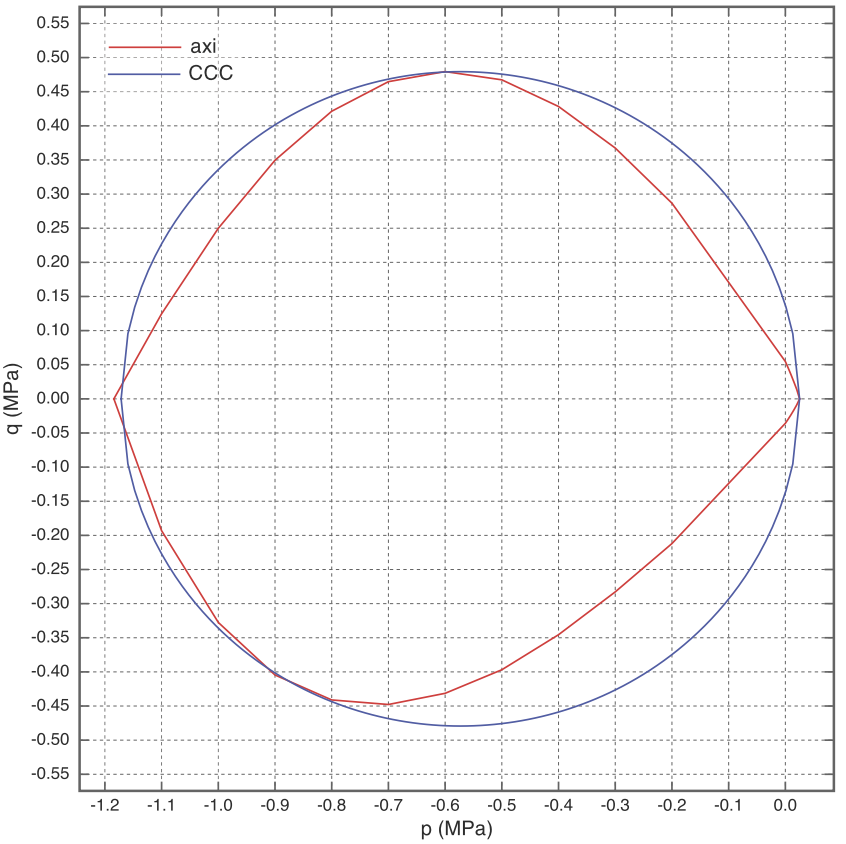

Fig. 5. The CCC criterion and the porous Coulomb criterion (axisymmetric code) – $c_m = 0.04027$ MPa, $\phi_m = 39.4178°$, $f = 0.25$.

It is worth noting that it is also possible to define the CCC criterion from the porosity and the Casagrande shear test by using the parametric form of the macroscopic porous Coulomb criterion proposed in the reference [10] and confirmed in [3] with the axisymmetric mixed code used here. For identification of the CCC criterion without this mixed code, the values of $\Sigma_{eq} = |Q_2| = q$ at the critical point ($\dot{q_1} = 0$) are given in the appendix for a wide range of porosities f and friction angles ϕ_m.

6. Implementation of the CCC criterion in plane strain LA methods

Using the static and mixed methods in plane strain usually needs to define the corresponding expression of the CCC criterion $g(\sigma)$ in the elements and in the Mohr plane for the velocity discontinuities from the three-dimensional expression (8). This is not necessary for the model of Fig. 1 when using the generalized plane strain codes of [15] (without the macroscopic variables Σ_i and D_i), since $d_{yz} = 0 = \partial g/\partial\sigma_{yz} \Rightarrow \sigma_{yz} = 0$ from (8) or (10), $d_{zx} = 0 \Rightarrow \sigma_{zx} = 0$ for the triangles. Similarly $\sigma_{tz} = \sigma_{zn} = 0$ for the velocity discontinuity sides in their (n, t, z) frames, with the same expression of g owing to the isotropy of the material. Finally, leaving σ_z under only $g(\sigma) \leq 0$ in the present optimization problems is equivalent to seeking the projection of the plastically admissible stress domain along the σ_z axis, i.e. $\partial g/\partial\sigma_z = 0 = d_z$. Hence, the problem is well modelized in plane strain. From the same reasoning, leaving σ_z and σ_t free (appearing only in the criterion) is equivalent to use the CCC expression in the Mohr plane for the velocity discontinuities in plane strain.

6.1. The kinematic mixed method

6.1.1. General formulation

The mixed formulation experienced in [16] and [17] for homogeneous von Mises and Gurson materials is here modified as follows, for a given vector U^d:

$$\max_{Q,\,\sigma,\,T'} U^d \cdot Q_L \tag{11.i}$$

$$\text{s.t.} \int_\Omega d(u) : \sigma \, d\Omega + \int_{S_d} [u] \cdot T' \, dS = U \cdot Q_L, \quad \forall u \, KA \tag{11.ii}$$

$$g(\sigma) \leq 0; \quad g_{nt}(T') \leq 0 \tag{11.iii}$$

where σ is related to the continuous material (of volume Ω), and T' to the discontinuity lines in their (n,t) frames. S_d is the union of the velocity discontinuity surfaces. The vector U is defined as (V_N, V_F) respectively associated with the loading vector $Q_L = (N, F)$; $g_{nt}(T')$ is the projection of $g(\sigma')$ on the Mohr plane associated with the discontinuity surface of normal n.

The plastic conditions also involve the interface stress conditions for the considered sides of the boundary, together with the CCC condition in their respective ntz frames. Hence, the intersection of the admissible stress domains of the metal, the interface itself and the material is realized. More precisely, the smooth interfaces along the parts with Teflon induce the supplementary linear conditions $\sigma_n \leq 0, \tau_{nt} = 0$. The loading plate is assumed perfectly rough and the corresponding stress vector under the plate is only limited by the soil criterion for this compressive problem.

In (11), the velocity field u must be kinematically admissible (KA), i.e. piecewise continuous with bounded discontinuities (such a feature is verified by the FEM velocity field), together with verifying the velocity conditions on the boundary and the loading U^{d}. It can be seen in the above-mentioned papers that the *optimal* velocity field will also be P.A. (plastically admissible), i.e. in the optimal solution the stress tensors σ or the stress vectors T' are associated with the strain rate tensor $d(u)$ or with the velocity jump $[u]$ by the normality law corresponding to $g(\sigma) = 0$ or $g_{nt}(T') = 0$, respectively.

6.1.2. Numerical implementation

The present mixed kinematic code involves four stress variables, i.e. $\sigma_x, \sigma_y, \sigma_z, \sigma_{xy}$ for each element as in [15], and $\sigma'_n, \sigma'_t, \sigma'_z, \sigma'_{nt}$ for each end of the discontinuity (and interface) sides, with σ'_z only appearing in the plasticity criterion, idem also for σ'_t. The usual admissibility conditions are similar to the ones in [15], excepting the criterion which is given by (10) (Σ becoming σ) for σ and σ', with $Q_4 = Q_5 = 0$. Finally, the numerical form of the mixed problem (11) becomes:

$$\begin{aligned} &\text{Max } \{U^{\mathrm{d}}\}^{\mathsf{T}}\{Q_L\} \\ &\text{s. t. } -[\alpha]\{\sigma\} - [\alpha']\{\sigma'\} + [\beta]\{Q_L\} = 0 \\ &\quad g_{xyz}(\sigma) \leq 0 \quad \forall \sigma; \; g_{ntz}(\sigma') \leq 0 \quad \forall \sigma' \\ &\quad + \text{KA velocity conditions} \end{aligned} \tag{12}$$

where σ is related to the finite elements (in the (x, y, z) frame), and σ' to the discontinuity sides in their (n, t, z) frames. In (12), the vector U is defined as (V_N, V_F), respectively, associated with the loading vector $Q_L = (N, F)$; from the isotropy of the material, the CCC criterion g_{ntz} has the same expression than g_{xyz}.

As shown in the detailed analysis of [16] and [17], we can identify the dual variables (associated with the linear constraints of the problem) of the optimal solution with the velocity components. This analysis also details how the resulting velocity field is plastically admissible; how the KA character of the optimal velocity field is ensured is explained in the following example.

We previously defined two supplementary rows (constraints) whose associated virtual variables are V_N, V_F and two new columns for the components N and F of the loading vector Q_L. For example, at each "vertex" in the metal parts of the lower half-box, we have to impose the conditions $u_x - V_F = 0$. This is done by adding one additional column (i.e. an additional variable for each condition); in this new column, we impose 1 and -1 at the row positions corresponding to u_x and V_F. The required condition will be verified in the optimal solution (from the so-called KKT optimality conditions), since the additional variable does not appear in the functional: see [18] for more details.

The final mixed problems is solved by using the "rotated quadratic" (conic) algorithm of the code MOSEK, and the solution is obtained in about one minute.

6.2. The static method

The static code is of the same type than in Section 3.2 by adding σ_z to the three components of the stress tensors. The criterion $g(\sigma)$ is now defined by (10) (with M numerically defined) after expressing the remaining components Q_1, Q_2, Q_3 and Q_6 (Σ becoming σ), σ_z being limited only by the criterion as in the mixed method; the final conic problem is also solved with MOSEK.

7. Numerical results with the CCC criterion

Fig. 6 gives the deformed meshes when using the same finite element discretization as in the Coulomb case, for the first and the third experimental values of N on the plate.

- Here also the optimal static and kinematic bounds are quasi-identical, the material in the two half-boxes remains undeformed, and the stress vector given by the static code is quasi-constant along the interface between the half-boxes.
- Here also the plastic flow appears only at the interface between the half-boxes, but the velocity jump depends on the vertical force; this jump becomes zero for $N = 280.9$ kN (see Table 4), i.e. for the so-called critical point of a Cam–Clay criterion (or the top point of the ellipse).

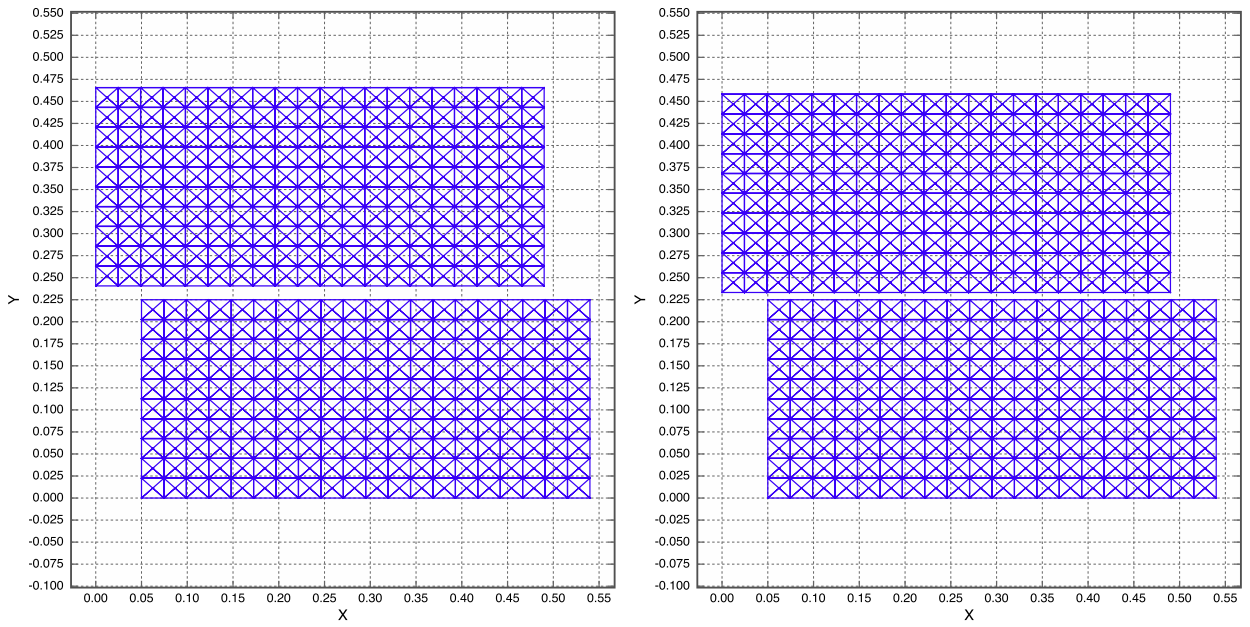

Fig. 6. Deformed meshes for $N1$ and $N3$ loadings, CCC material.

Table 4
The numerical and experimental limit loads.

N (kN)	78.4	117.6	156.8	280.89
F_{exp} (kN)	70.3	98.05	125.8	–
F_{MEF} (kN)	107.55	118.12	125.797	135.61

The horizontal optimal forces are given as F_{MEF} in Table 4 for the three experimental loadings N_i: only the third loading F_{exp} is a limit loading (or collapse load) in the sense of LA, as expected. As expected also from the constancy of the stress vector on GH, it can be verified (by dividing by the length of GH, i.e. 0.49 m), that the values of the CCC tangential stress of Table 3 are practically retrieved (after conversion to MPa units).

Let us recall here that the CCC criterion is defined in such a way that the three results are admissible, and that they are upper bounded as closely as possible. Hence, from the non-linearity of the CCC (as it can be seen also in Fig. 4), the experimental values are significantly lower than the FEM results for the N1 test and, in a less extent, for the N2 test.

8. Analysis and conclusion

In a preliminary study of the Casagrande shear test where the rammed earth is considered as a Coulomb material, the numerical static and kinematic approaches of Limit Analysis give quasi-identical results, resulting in the exact solution with a two-block kinematics; both stress vector and velocity jump are constant along the shearing plane. However, this dilatancy is not depending on the intensity of the vertical loading for a given imposed horizontal velocity, a questionable feature when considering the non-negligible porosity of the material.

As an attempt to take into account this porous character, an elliptic approximation of the porous Coulomb criterion, here called Cohesive Cam–Clay (CCC), is fully defined by using theoretical results and recent codes for solving the homogenization problem resulting from the hollow sphere model. In a second step, with this CCC criterion, both static and mixed LA codes are developed and used for the Casagrande problem. Using these codes, the velocity jump at the shearing interface depends this time on the intensity of the compressive force on the upper box. Here also, the plastic flow occurs only at the shearing interface, and the corresponding stress vector appears quasi-constant all along this interface.

Nevertheless, the CCC criterion is not entirely satisfactory regarding the observed jump in the tests and also the numerical results for the first tests versus the experimental ones. To refine this CCC evaluation, complementary experimental tests beyond the last (and maximal) loading point of Fig. 2 should be necessary, such tests being unfortunately not structurally possible with the apparatus used here. For example, in an attempt to verify the maximal compressive normal stress of Fig. 4, the confined compression test (i.e. without horizontal loading), should need a vertical loading at least four times more than the last experimental point.

However, the CCC criterion takes into account the influence of the porosity of the material *via* the hollow sphere model. On the other hand, the FEM solutions based on the CCC criterion can be considered as very good approximations of the solution with the homogenized material fully defined from the hollow sphere model. These two FEM codes with the CCC

Table 5
Σ_{eq} at the critical point for porosity f and friction angle ϕ_m given by the mixed kinematic code – $c_m = 1$.

ϕ_m (°) \ f	0.05	0.10	0.15	0.20	0.25	0.30
2.5	1.91544	1.77051	1.65295	1.54504	1.44224	1.34071
5	2.04007	1.85045	1.71289	1.59359	1.48254	1.37603
7.5	2.26193	1.96147	1.79347	1.65739	1.53468	1.41976
10	2.60234	2.13308	1.90082	1.73734	1.59970	1.47311
12.5	3.09768	2.38643	2.05216	1.84195	1.67912	1.53728
15	3.82041	2.74722	2.26916	1.98385	1.78115	1.61660
17.5	4.87931	3.25514	2.57313	2.18009	1.91662	1.71660
20	6.50814	3.98269	2.99596	2.45270	2.09972	1.84680
22.5	9.04628	5.04671	3.59306	2.82982	2.35103	2.01978
25	13.2917	6.65700	4.45433	3.35634	2.69738	2.25545
27.5	20.6474	9.18097	5.72973	4.11270	3.18065	2.57940
30	34.5160	13.3363	7.70056	5.22414	3.87225	3.03103
32.5	62.3208	20.5854	10.8680	6.92574	4.88806	3.67751
35	123.895	34.1423	16.2647	9.64514	6.43975	4.63271
37.5	276.748	61.6884	26.1073	14.2481	8.92369	6.09469
40	713.310	123.608	45.5840	22.5939	13.1411	8.45033

criterion are original and powerful tools for computing limit loads of structures involving the porous Coulomb material recently defined in [10,3].

To go further about rammed earth structures with direct methods, we could consider a non-standard approach where the Coulomb plasticity criterion and the flow potential are different, even if, in this case, the computed loading is not guaranteed as a limit load, and if unicity theorems available in the LA framework are lost. A first solution to obtain that the three experimental loadings be retrieved—together with the absence of dilatation jump observed in the experimental tests—might be to use the results of Drescher and Detournay in [19], but this approach is limited to translational velocity mechanisms only.

A more general approach would be the implicit standard approach introduced by G. de Saxcé [20] to attempt to extend the theorems of limit analysis to non-standard materials, based on a bipotential function specific of the material. However, a general bipotential function for the Coulomb material is not presently available, even if such a function for the discontinuities has been defined in a recent study [21]; the method is then limited, for the moment, to rigid block mechanisms.

Another interesting option could be the use of the implicit standard framework for the CCC material, as in the very complete work [22] based on the bifunctional given also by de Saxcé in [23] for the Modified Cam–Clay material with hardening. However, for non-hardening materials as here, the corresponding bifunctional for the CCC criterion, or for the criterion of the same form in [13] or [14], is not presently available in the literature.

Appendix A. Σ_{eq} values for $\mathrm{tr}(\boldsymbol{d}) = 0$ from the axisymmetric code of [3]

To obtain the Σ^0_{eq} value for a cohesion c^0 from Σ_{eq} given in Table 5: $\Sigma^0_{eq} = c^0\,\Sigma_{eq}$.

References

[1] P. Thoré, F. Pastor, J. Pastor, D. Kondo, Closed form solutions for the hollow sphere model with Coulomb and Drucker–Prager materials under isotropic loadings, C. R. Mecanique 337 (2009) 260–267.
[2] J. Pastor, P. Thoré, F. Pastor, Limit analysis and numerical modeling of spherically porous solids with Coulomb and Drucker–Prager matrices, J. Comput. Appl. Math. 234 (2010) 2162–2174.
[3] F. Pastor, K. Anoukou, J. Pastor, D. Kondo, Limit analysis and homogenization of porous materials with Mohr–Coulomb matrix. Part II: Numerical bounds and assessment of the theoretical model, J. Mech. Phys. Solids 91 (2016) 14–27.
[4] MOSEK ApS, C/O Symbion Science Park, Fruebjergvej 3, Box 16, 2100 Copenhagen ϕ, Denmark, http://www.mosek.com, 2010.
[5] R. El-Nabouch, Q.-B. Bui, N. Prime, P. Perrotin, O. Plé, Comportement de murs en pisé sous poussée progressive : étude expérimentale et numérique, Rencontres Universitaires de Génie Civil, 2016.
[6] R. El-Nabouch, Mechanical Behavior of Rammed Earth Walls Under Pushover Tests, Thèse de doctorat de la communauté université Grenoble Alpes, Université Savoie Mont Blanc, June 2017.
[7] J. Pastor, Analyse limite : détermination numérique de solutions statiques complètes. Application au talus vertical, J. Méc. Appl. (now Eur. J. Mech. A, Solids) 2 (1978) 167–196.
[8] R. Abdi, P. de Buhan, J. Pastor, Calculation of the critical height of a homogenized reinforced soil wall: a numerical approach, Int. J. Numer. Anal. Methods Geomech. 18 (1994) 485–505.
[9] A.L. Gurson, Continuum theory of ductile rupture by void nucleation and growth – part I: Yield criteria and flow rules for porous ductile media, J. Eng. Mater. Technol. 99 (1977) 2–15.
[10] K. Anoukou, F. Pastor, P. Dufresnoy, D. Kondo, Limit analysis and homogenization of porous materials with Mohr–Coulomb matrix. Part I: Theoretical formulation, J. Mech. Phys. Solids 91 (2016) 145–171.
[11] A. Schofield, A. Wroth, Critical State Soil Mechanics, McGraw-Hill, 1968.
[12] K.H. Roscoe, J.H. Burland, On the generalized stress-strain behaviour of wet clay, in: J. Heyman, J. Leckie (Eds.), Engineering Plasticity, 1968.
[13] E.E. Alonso, A. Gens, A. Josa, A constitutive model for partially saturated soils, Géotechnique 40 (3) (1990) 405–430.
[14] R.I. Borja, Cam–clay plasticity. Part V: A mathematical framework for three-phase deformation and strain localization analyses of partially saturated porous media, Comput. Methods Appl. Mech. Eng. 193 (2004) 5301–5338.

[15] F. Pastor, J. Pastor, D. Kondo, Numerical limit analysis and plasticity criterion of a porous Coulomb material with elliptic cylindrical voids, C. R. Mecanique 343 (2015) 199–200.
[16] F. Pastor, Résolution par des méthodes de point intérieur de problèmes de programmation convexe posés par l'analyse limite, Thèse de doctorat, Facultés universitaires Notre-Dame de la Paix, Namur, Belgium, 2007.
[17] F. Pastor, E. Loute, J. Pastor, M. Trillat, Mixed method and convex optimization for limit analysis of homogeneous Gurson materials: a kinematical approach, Eur. J. Mech. A, Solids 28 (2009) 25–35.
[18] F. Pastor, D. Kondo, J. Pastor, 3D-FEM formulations of limit analysis methods for porous pressure-sensitive materials, Int. J. Numer. Methods Eng. 95 (2013) 847–870.
[19] A. Drescher, E. Detournay, Limit load in translational materials for associated and non-associated materials, Géotechnique 43 (1993) 443–456.
[20] G. de Saxcé, Une généralisation de l'inégalité de Frenchel et ses applications aux lois constitutives, C. R. Acad. Sci. 314 (1992) 125–129.
[21] M. Hamlaoui, A. Oueslati, G. de Saxcé, A bipotential approach for plastic limit loads of strip footings with non-associated materials, Int. J. Non-Linear Mech. 90 (2017) 1–10.
[22] N. Zouain, I.P. Filho, L. Borges, L.M. da Costa, Plastic collapse in non-associated hardening materials with application to Cam–clay, Int. J. Solids Struct. 44 (2007) 4382–4398.
[23] G. de Saxcé, The bipotential method, a new variational and numerical treatment of the dissipative laws of materials, in: 10th Int. Conf. on Mathematical and Computer Modelling and Scientific Computing, Boston, MA, USA, 1995.